Hybrid Control of DC–DC Series Resonant Converters: The Direct Piecewise Affine Approach

Hamed Molla-Ahmadian, Farzad Tahami, *Senior Member, IEEE*, Ali Karimpour, and Naser Pariz

***Abstract*—The control and stabilization of resonant converters are essential problems in power electronics. The conventional controller design and stability analysis for these converters are based on the linearized averaged model. Nevertheless, the state variables in resonant converters have large ac variations and the validity of the linearized average model is violated. Hence, using large signal and nonaveraged models are necessary for controller design and stability analysis. In this paper, a new hybrid controller is presented that is applicable to dc–dc series resonant converters and use neither averaging nor small signal approximation. The dc–dc resonant converters are inherently switched affine systems with constrained switching law. The proposed controller is based on the switched behavior of the converter and the concept of piecewise affine methodology. Moreover, it has switched inner and proportional-integral (PI) outer control loops and does not require a modulator. The large signal and closed loop stability analysis of the resonant converters is presented by a theorem. The minimum phase attribute of the control system is investigated by zero dynamic stability analysis. The proposed controller has less complexity in comparison to other suggested controllers and can be implemented using simple analog circuits. The simulation and experimental results show the effectiveness of the proposed method.**

***Index Terms*—Hybrid control, hybrid modeling, piecewise affine systems, resonant converter.**

I. Introduction

NOWADAYS, using high-frequency power converters is inevitable in many applications. The switching losses and electromagnetic interferences are major issues in these converters. Resonant converters can overcome these restrictions by using zero current and/or voltage switching.

Due to the large ac variations in currents and voltages of the resonant tank, the linearized model of the resonant converters has considerably large modeling error. This phenomenon makes the control of resonant converters more complex than pulse width modulation (PWM) converters. Due to sinusoidal approximation along with averaging and small signal approximation, the conventional controller design and stability analysis of resonant converters involve considerable error and limitations. Consequently, sophisticated control techniques with solid stability analysis are necessary. On the other hand, the accuracy of the small signal model and the designed controller diminish while the load resistance or the input voltage source have large variations. Therefore, it is essential to investigate the stability of the resonant converters using a nonlinear model.

The nonlinear analysis and controller design of the resonant converter were presented in [1] and [2]. The nonlinear stability analysis of the resonant converters has been investigated in [3]. Nevertheless, the stability analysis and controller design of nonlinear dynamics are complex and there is no systematic approach for stability analysis of these types of converters in general. The piecewise affine (PWA) or piecewise linear (PWL) approximation of nonlinear averaged model are solutions for this problem. These methods have been applied to nonlinear averaged model of dc–dc PWM converters [4], power factor correction rectifiers [5], and quasi-resonant converters [6]. Because of the large ac variations of resonant tank variables, using these methods on nonaveraged model of the resonant converters is not acceptable.

A hybrid flatness approach was presented in [7] which is based on the nonaveraged model of the converter and passivity-based control. The robust performance and stability are the limitations of this paper. The switched control of a three-phase PWM rectifier was presented in [8]. Optimal state feedback control of PWM dc–dc converters is presented in [9] which guarantees the region of stability. The large signal stability of the buck converter was given in [10] which provides a fixed frequency hysteresis controller by using Filippov method and Floquet theory. This method uses the averaging and defines the region of stability. In [11], the mixed control of *LLC* resonant inverter is presented based on frequency and duty cycle control for steady state and transient responses, respectively.

In this paper, a new class of hybrid systems is presented for hybrid modeling and control of resonant converters . Since the presented class is similar to PWA systems and it is derived directly from switched model of converter, it is called direct PWA (DPWA). The DPWA modeling of the resonant converters was first presented by the authors in [12]. In this paper, using DPWA modeling technique, the closed loop stability analysis, the minimum phase exhibit of control system, and controller design for a dc–dc series resonant converter is presented. The hybrid control of a dc–dc resonant converter is performed by

Manuscript received August 29, 2013; revised December 5, 2013 and February 27, 2014; accepted April 13, 2014. Date of publication July 1, 2014; date of current version October 15, 2014. This work was supported in part by the Department of Electrical Engineering, Ferdowsi University of Mashhad, Mashhad, Iran. Recommended for publication by Associate Editor V. Agarwal.

H. Molla-Ahmadian was with the Department of Electrical Engineering, Ferdowsi University of Mashhad, 9177948974 Mashhad, Iran. He is now with the Department of Electrical Engineering, Khorasan Institute of Higher Education, 9189893661 Mashhad, Iran (e-mail: mollaahmadian@khorasan.ac.ir).

F. Tahami is with the Department of Electrical Engineering, Sharif University of Technology, 1115511365 Tehran, Iran (e-mail: tahami@sharif.ir).

A. Karimpour and N. Pariz are with the Department of Electrical Engineering, Ferdowsi University of Mashhad, 9177948974 Mashhad, Iran (e-mail: karimpor@um.ac.ir; n-pariz@um.ac.ir).

Color version of one or more of the figures in this paper are available online at http://ieeexplore.ieee.org.

Digital Object Identifier 10.1109/TPEL.2014.2320958

an adaptive switching strategy. This strategy comprises of two different inner and outer control loops that are switched and PI control loops, respectively. The inner loop controls the transient response and the outer loop regulates the steady-state response. The inner control loop has a large bandwidth that it is close to the switching frequency. The outer control loop has a small bandwidth that it is about the inverse of output filter time constant. On the other hand, the outer loop adapts the specifications of the inner loop. The associated closed loop stability analysis is also addressed, and, furthermore, a switched control strategy is presented for control of DPWA model of converter which can overcome the main limitations of the conventional control approaches. The presented approach has simple structure which does not require a modulator and is implemented by simple analog circuits. The estimation of tank capacitor voltage is done by using integrator and current sensing circuits. The simulation and experimental results show the effectiveness of the proposed method.

The main contributions of this paper are as follows: 1) a new hybrid control strategy is presented which does not require a modulator, 2) the control strategy for the hybrid model of the dc–dc series resonant converter (SRC) is introduced and the closed loop system is formulated in DPWA form, 3) the closed loop and zero dynamic stability analysis of the proposed method is presented, 4) the proposed method uses the advanced theories of hybrid control systems but they could be implemented by simple analog circuits.

This paper is organized as follows. In Section II, the switched systems is introduced. The DPWA model of dc–dc SRC is derived in Section III. In Section IV, the DPWA controller for dc–dc SRC is presented. A case study with simulation results for verification of the proposed model are presented in Section V. Section VI demonstrates the experimental implementation of the proposed control strategy and discusses the results. Finally, the conclusion of the paper is presented in Section VII.

II. Switched Systems

In this section, two types of switched systems are introduced which will be used in the presented modeling approach.

A. PWA Models

A model of continuous hybrid systems is given by [13]

$$\begin{cases} \dot{x}(t) = f(x(t), i(t), u(t)) \\ y(t) = g(x(t), i(t), u(t)) \\ i(t^+) = \varphi(x(t), i(t), u(t), s(t)) \end{cases} \tag{1}$$

where $i(t) \in \{1, 2, \ldots, M\}, u(t) \in R, s(t) \in \{0, 1\}, y(t) \in R$, and $x(t) \in R^n$ are subsystem index number, control input, logic-input, output and state variables, respectively, M is the number of the subsystems and φ is the switching law. Many classes of hybrid systems are extended for different applications. Switching among subsystems may be free or constrained.

A well-known class of hybrid systems is the class of piecewise affine (PWA) systems which can be developed for many applications. The stability analysis and controller design of PWA systems have been investigated in [14]–[16]. The mathematical description of a PWA system is

$$\begin{cases} \dot{x} = A_i x + B_i u + b_i, & \text{if}: x \in \Omega_i \\ y = Cx \end{cases} \tag{2}$$

such that $\Omega_i \cap \Omega_j = \phi, i \neq j$ and $\cup_{i=1}^{M} \Omega_i = R^n$, $x \in R^n$, M is the number of subsystems or equivalently cells and i and j are the subsystem index numbers. The state space may be partitioned as polytopic or ellipsoidal cells. The mathematical description of cells are as follows:

$$\Omega_i = \bigcap_{j=1}^{p_i} \{\, x \in R^n \;\mid\; h_{ij}^T x - g_{ij} < 0 \,\} \tag{3}$$

or

$$\Omega_i = \bigcap_{j=1}^{p_i} \{\, x \in R^n \;\mid\; x^T H_{ij}^T x - g_{ij} < 0 \,\} \tag{4}$$

where h_{ij} and g_{ij} are constant vectors, H_{ij} is the constant matrix which defines the *i*th cell boundary, p_i is number of surfaces or curves boundaries that describe the *i*th cell.

B. DPWA Models

The DPWA is derived from extension of conventional PWA into switched systems [12]. The mathematical representation of this class is

$$\begin{cases} \dot{x} = A_i x + b_i \\ y = Cx. \end{cases} \tag{5}$$

The subscript i is the index of cell in which the state trajectory lies in. The cells may have polyhedral or ellipsoidal boundaries. The cell description is as follows:

$$\Omega_i = \bigcap_{j=1}^{p_i} \{\, x \in R^n \;\mid\; (h_{ij}^T + h_{ij}^{*\,T}) x - g_{ij} < 0 \,\} \tag{6}$$

for polyhedral type or

$$\Omega_i = \bigcap_{j=1}^{p_i} \{\, x \in R^n \;\mid\; x^T (H_{ij} + H_{ij}^*) x - g_{ij} < 0 \,\} \tag{7}$$

for ellipsoidal type. The h_{ij} and H_{ij} contain the constant elements and h_{ij}^* and H_{ij}^* include the variable parameters. A simple graphical representation of DPWA systems with polyhedral cells is presented in Fig. 1. The tunable boundaries cause the nonautonomous switching and the inherent and nontunable boundaries make the autonomous switching. The cell boundaries in PWA systems are fixed, while in DPWA systems, the boundaries are a combination of constant and variable constraints. DPWA systems are appropriate for modeling of power electronic converters such as resonant converters.

III. DPWA Modeling of DC–DC SRC

A dc–dc SRC is shown in Fig. 2. In this figure, x_1, x_2, and x_3 are the current of the tank inductor, the voltage of the tank capacitor, and the voltage of the filter capacitor, respectively. V_s

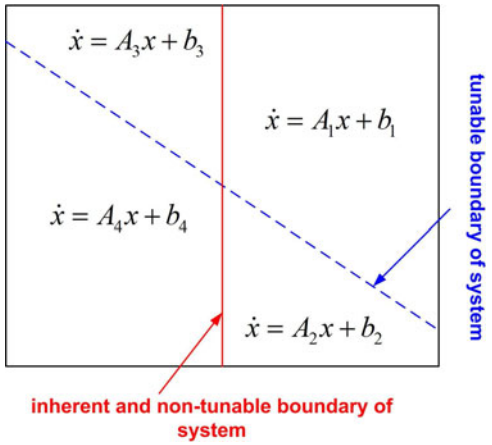

Fig. 1. Simple graphical representation of DPWA systems with four polyhedral cells.

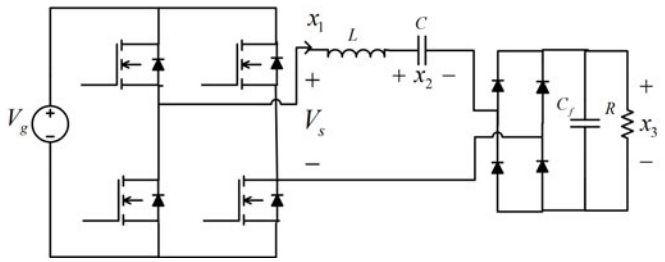

Fig. 2. DC–DC series resonant converter.

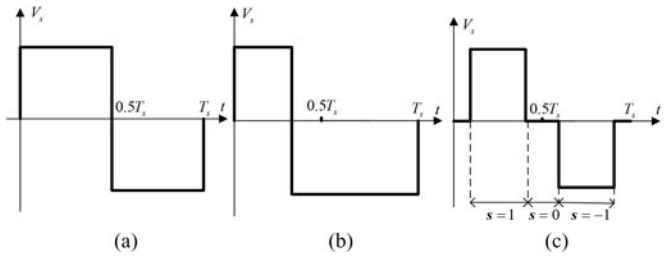

Fig. 3. Waveform of V_s for different control strategies: (a) frequency, (b) asymmetrical duty cycle, (c) symmetrical duty cycle.

is the output voltage of the MOSFET bridge. Assuming that the converter operates in continuous conduction mode (CCM), the nonlinear model of the converter is described by [12]

$$\begin{cases} \dfrac{dx_1}{dt} = \dfrac{1}{L}\left\{sV_g - x_2 - r_{\text{Loss}}x_1 - \text{sign}(x_1)(x_3 + 2V_f)\right\} \\ \dfrac{dx_2}{dt} = \dfrac{1}{C}(x_1) \\ \dfrac{dx_3}{dt} = \dfrac{1}{C_f}\left(|x_1| - \dfrac{x_3}{R}\right) \end{cases} \tag{8}$$

where V_f is the forward voltage drop of output diodes, r_{Loss} is the sum of the inductor resistance and the capacitor series resistance, and $s \in \{-1, 0, +1\}$ is the logic-input that defines the state of the input switches. Fig. 3 shows the output voltage

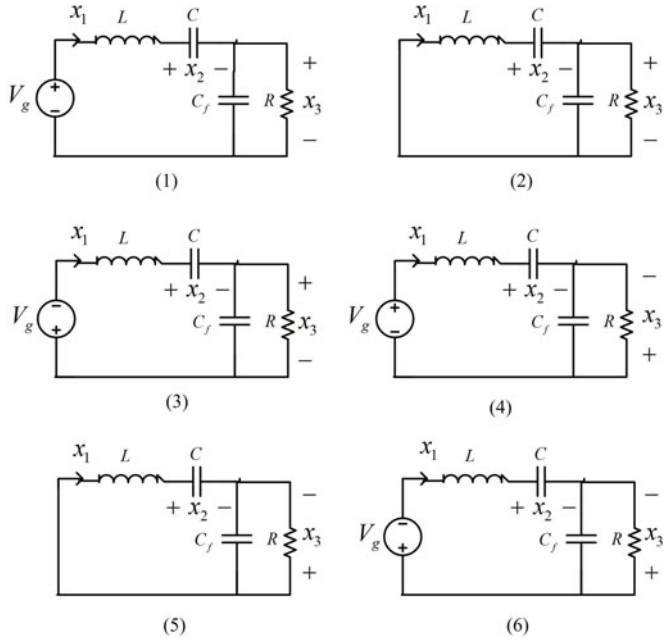

Fig. 4. Six modes of dc–dc SRC with following conditions as: (1) $x_1 > 0$, $s = 1$, (2) $x_1 > 0$, $s = 0$, (3) $x_1 > 0$, $s = -1$, (4) $x_1 < 0$, $s = 1$, (5) $x_1 < 0$, $s = 0$, (6) $x_1 < 0$, $s = -1$.

of the MOSFET bridge V_s for different control strategies. The proposed method is not among the conventional control strategies but can be considered as a combination of frequency and symmetrical duty cycle control strategies. The control signal of proposed modeling is direct gate signal of MOSFETs.

Since the sign and the absolute value functions are hard nonlinear, this model defined by (8) is not appropriate for stability analysis. Furthermore, there is no straightforward relation between frequency or duty cycle with state variables.

The dc–dc SRC is naturally a switched system with affine subsystems. Depending on semiconductor states, six modes and subsystems may be occurred. The modes are shown in Fig. 4 for different conditions.

The logic input s is defined as follows for transforming the constrained switched affine model to DPWA model

$$s = \begin{cases} +1 & Kx + m > \gamma \\ 0 & \gamma \geq Kx + m > -\gamma \\ -1 & -\gamma \geq Kx + m \end{cases} \tag{9}$$

where $K = [k_1\ k_2\ k_3], m$ and γ are the parameters of switching surfaces that define the s variable.

The DPWA model of dc–dc SRC is described by

$$\begin{cases} \dot{x}(t) = \mathbf{A}_i x(t) + \mathbf{b}_i \\ y(t) = \mathbf{C}x(t) \\ i = \varphi(x(t)) \end{cases} \tag{10}$$

TABLE I
DIFFERENT SUBSYSTEMS OF DC–DC SRC MODEL THAT IS DESCRIBED IN (10) AND PRESENTED IN FIG. 4

i	A_i	b_i	conditions
1	$\begin{bmatrix} \frac{-r_{\text{Loss}}}{L} & \frac{-1}{L} & \frac{-1}{L} \\ \frac{1}{C} & 0 & 0 \\ \frac{1}{C_f} & 0 & \frac{-1}{C_f R} \end{bmatrix}$	$\begin{bmatrix} \frac{V_g - 2V_f}{L} \\ 0 \\ 0 \end{bmatrix}$	$x_1 > 0,$ $s = 1$
2	$\begin{bmatrix} \frac{-r_{\text{Loss}}}{L} & \frac{-1}{L} & \frac{-1}{L} \\ \frac{1}{C} & 0 & 0 \\ \frac{1}{C_f} & 0 & \frac{-1}{C_f R} \end{bmatrix}$	$\begin{bmatrix} \frac{-2V_f}{L} \\ 0 \\ 0 \end{bmatrix}$	$x_1 > 0,$ $s = 0$
3	$\begin{bmatrix} \frac{-r_{\text{Loss}}}{L} & \frac{-1}{L} & \frac{-1}{L} \\ \frac{1}{C} & 0 & 0 \\ \frac{1}{C_f} & 0 & \frac{-1}{C_f R} \end{bmatrix}$	$\begin{bmatrix} \frac{-V_g - 2V_f}{L} \\ 0 \\ 0 \end{bmatrix}$	$x_1 > 0,$ $s = -1$
4	$\begin{bmatrix} \frac{-r_{\text{Loss}}}{L} & \frac{-1}{L} & \frac{1}{L} \\ \frac{1}{C} & 0 & 0 \\ \frac{-1}{C_f} & 0 & \frac{-1}{C_f R} \end{bmatrix}$	$\begin{bmatrix} \frac{V_g + 2V_f}{L} \\ 0 \\ 0 \end{bmatrix}$	$x_1 < 0,$ $s = 1$
5	$\begin{bmatrix} \frac{-r_{\text{Loss}}}{L} & \frac{-1}{L} & \frac{1}{L} \\ \frac{1}{C} & 0 & 0 \\ \frac{-1}{C_f} & 0 & \frac{-1}{C_f R} \end{bmatrix}$	$\begin{bmatrix} \frac{2V_f}{L} \\ 0 \\ 0 \end{bmatrix}$	$x_1 < 0,$ $s = 0$
6	$\begin{bmatrix} \frac{-r_{\text{Loss}}}{L} & \frac{-1}{L} & \frac{1}{L} \\ \frac{1}{C} & 0 & 0 \\ \frac{-1}{C_f} & 0 & \frac{-1}{C_f R} \end{bmatrix}$	$\begin{bmatrix} \frac{-V_g + 2V_f}{L} \\ 0 \\ 0 \end{bmatrix}$	$x_1 < 0,$ $s = -1$

TABLE II
MATRICES OF H_i AND g_i OF (11) WITH $K = [k_1\ k_2\ k_3]$

i	H_i	g_i
1	$\begin{bmatrix} -1 & 0 & 0 \\ -k_1 & -k_2 & -k_3 \\ 0 & 0 & 0 \end{bmatrix}$	$\begin{bmatrix} 0 & -\gamma + m & 0 \end{bmatrix}^T$
2	$\begin{bmatrix} -1 & 0 & 0 \\ -k_1 & -k_2 & -k_3 \\ k_1 & k_2 & k_3 \end{bmatrix}$	$\begin{bmatrix} 0 & \gamma + m & \gamma - m \end{bmatrix}^T$
3	$\begin{bmatrix} -1 & 0 & 0 \\ 0 & 0 & 0 \\ k_1 & k_2 & k_3 \end{bmatrix}$	$\begin{bmatrix} 0 & 0 & -\gamma - m \end{bmatrix}^T$
4	$\begin{bmatrix} 1 & 0 & 0 \\ -k_1 & -k_2 & -k_3 \\ 0 & 0 & 0 \end{bmatrix}$	$\begin{bmatrix} 0 & -\gamma + m & 0 \end{bmatrix}^T$
5	$\begin{bmatrix} -1 & 0 & 0 \\ -k_1 & -k_2 & -k_3 \\ k_1 & k_2 & k_3 \end{bmatrix}$	$\begin{bmatrix} 0 & \gamma + m & \gamma - m \end{bmatrix}^T$
6	$\begin{bmatrix} -1 & 0 & 0 \\ 0 & 0 & 0 \\ k_1 & k_2 & k_3 \end{bmatrix}$	$\begin{bmatrix} 0 & 0 & -\gamma - m \end{bmatrix}^T$

where A_i and b_i are shown in Table I and $\mathbf{C} = [\,0 \quad 0 \quad 1\,]$ and i is

$$\varphi(x(t)) = \begin{cases} 1 & H_1^T x - g_1 < 0 \\ 2 & H_2^T x - g_2 < 0 \\ 3 & H_3^T x - g_3 < 0 \\ 4 & H_4^T x - g_4 < 0 \\ 5 & H_5^T x - g_5 < 0 \\ 6 & H_6^T x - g_6 < 0 \end{cases} \tag{11}$$

where $H_i = [h_{i1}^T \ \ h_{i2}^T \cdots h_{ip_i}^T]^T$, $g_i = [g_{i1} \ \ g_{i2} \cdots g_{ip_i}]^T$ and they are defined in Table II. The state of $s = 0$ is equal to dead time state in switching among two switches.

IV. DPWA CONTROLLER FOR DC-DC SRC

The proposed strategy is based on DPWA model of Section III.

A. Adaptive Switched Controller: DPWA Controller

The proposed controller can be modeled as a DPWA system and it is denoted as DPWA controller. The block-diagram of the proposed control strategy is shown in Fig. 5. It includes two different control loops; the inner and the outer loops. The inner control loop has a large bandwidth that controls the transient regime and is a switched controller. The inputs of the switched controller are state variables x, dc offset of switching surface m, and the slope of switching surface image on $x_1 - x_2$ plane k, and the output of the switched controller is the logic input s. The mathematical representation of the switched controller is as follows:

$$s = \text{sign}(-kx_1 + x_2 + m) = \begin{cases} +1 - kx_1 + x_2 + m > 0 \\ -1 - kx_1 + x_2 + m < 0. \end{cases} \tag{12}$$

The outer control loop has small bandwidth that controls the steady-state regime and is a PI controller which adjusts the slope of switching surface image on $x_1 - x_2$ plane of the inner control loop. The input to the outer loop is the error e and its output is the k.

B. Closed Loop Stability Analysis

The closed loop stability analysis of the proposed control strategy is a critical problem which is addressed by the following theorem.

Theorem 1: Consider the hyperplane DPWA system

$$\begin{cases} \dot{x} = A_i x + b_i, & x \in \Omega_i \\ y = Cx \end{cases}$$

$$\Omega_i = \bigcap_{j=1}^{p_i} \{\, x \in R^n \ \mid \ (h_{ij}^T + h_{ij}^{*\,T})x - g_{ij} - \boldsymbol{m} < 0 \,\} \tag{13}$$

where h_{ij}^* and $\boldsymbol{m}$ are design variables. With the following PI controller

$$\begin{cases} \dot{z} = y_{\text{ref}} - y \\ k = k_I\, z + k_P\, (y_{\text{ref}} - y) \\ h_{ij}^* = [\,k \quad -1 \quad 0\,]^T \end{cases} \tag{14}$$

z is state variable of PI controller. If one can find a solution for the following LMIs then the closed loop system is globally

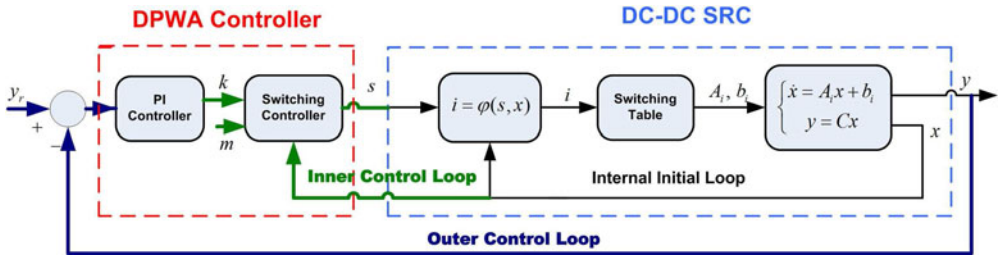

Fig. 5. Block-diagram of the proposed control strategy with the inner and the outer control loops.

stable

$$\boldsymbol{P} > 0 \tag{15}$$

$$A_{\text{aug},i}^T \boldsymbol{P} + \boldsymbol{P} A_{\text{aug},i} + \alpha_i \boldsymbol{P} + \sum_{j=1}^{p_i} \begin{bmatrix} 0 & 0 & 0 \\ 0 & 0 & 0 \\ 0 & 0 & \hat{\boldsymbol{m}}_{\boldsymbol{j}} \end{bmatrix}$$
$$- \sum_{j=1}^{p_i} \boldsymbol{\theta}_j \begin{bmatrix} -C^T \begin{bmatrix} 1 & 0 & 0 \end{bmatrix} & 0 & 0 \\ k_I \begin{bmatrix} 1 & 0 & 0 \end{bmatrix} & 0 & 0 \\ k_P\, y_{\text{ref}} \begin{bmatrix} 1 & 0 & 0 \end{bmatrix} - \begin{bmatrix} 0 & 1 & 0 \end{bmatrix} + h_{ij}^T & 0 & g_{ij} \end{bmatrix} < 0 \tag{16}$$

where

$$A_{\text{aug},i} = \begin{bmatrix} A_i & 0 & b_i \\ -C & 0 & y_{\text{ref}} \\ 0 & 0 & 0 \end{bmatrix} \tag{17}$$

k_I, k_P, and α_i are the constant parameters and y_{ref} is desired value of y. $\boldsymbol{P}, \hat{\boldsymbol{m}}_j$, and $\boldsymbol{\theta}_j$ are LMI variables. $\boldsymbol{m}$ is determined based on the intermediate variable $(\hat{\boldsymbol{m}}_j)$ which is defined as follows:

$$m = \frac{\hat{\boldsymbol{m}}_j}{\boldsymbol{\theta}_j}. \tag{18}$$

The proof of the *Theorem 1* is presented in Appendix . This theorem is used for closed loop stability analysis of DPWA models which can be solved by LMIs in the form of convex optimization problem.

C. Zero Dynamics of Controlled System

In this section, the stability analysis of the zero dynamics for dc–dc SRC is presented. The zero dynamics is defined to be the internal dynamics of the system when the system output is kept at zero by the input. The zero dynamics is a substantial feature of a nonlinear system, which does not depend on the controller or the desired trajectories [17]. The minimum phase response is a practical point for control systems. For studying the minimum phase attribute of control system, one must investigate the stability of the zero dynamics. The zero-dynamic stability analysis of power electronic converters are investigated in [18].

The zero dynamic of the control system is considered as $\hat{y} = y_{\text{ref}} - y = 0$ that $\hat{y}$ is defined as an auxiliary output variable. It is a minimum phase output subjected to the conditions that are presented in *Theorem 2*. Then, the dynamic of the closed loop system which is presented in (13) and (14) can be rewritten as

$$\begin{cases} \dot{x} = A_i x + b_i, & x \in \Omega_i \\ \hat{y} = y_{\text{ref}} - Cx = 0 \end{cases}$$
$$\Omega_i = \bigcap_{j=1}^{p_i} \{\, x \in R^n \mid ({h_{ij}^*}^T + h_{ij}^T)x - g_{ij} - \boldsymbol{m} < 0 \,\}$$
$$h_{ij}^* = \begin{bmatrix} k_I\, z_0 & -1 & 0 \end{bmatrix}^T \tag{19}$$

where z_0 is the initial value of z and is a constant value. The degree of (19) is n and it is less than the degree of main closed loop system. The stability of (19) is equivalent to zero dynamic stability as well as minimum phase attribute. The following theorem is presented for stability analysis of the zero dynamic of control system.

Theorem 2: Consider the hyperplane DPWA system (13) with the PI controller of (14). If one can find a solution for the following LMIs then the zero dynamic system is globally stable and the control system is minimum phase

$$\boldsymbol{P} > 0 \tag{20}$$

$$A_{\text{aug},i}^T \boldsymbol{P} + \boldsymbol{P} A_{\text{aug},i} + \alpha_i \boldsymbol{P} + \sum_{j=1}^{p_i} \begin{bmatrix} 0 & 0 \\ 0 & \hat{\boldsymbol{m}}_{\boldsymbol{j}} \end{bmatrix}$$
$$- \sum_{j=1}^{p_i} \boldsymbol{\theta}_j \begin{bmatrix} -C^T \begin{bmatrix} 1 & 0 & 0 \end{bmatrix} & 0 \\ \begin{bmatrix} k_I z_0 & -1 & 0 \end{bmatrix} + h_{ij}^T & -g_{ij} \end{bmatrix} < 0 \tag{21}$$

where

$$A_{\text{aug},i} = \begin{bmatrix} A_i & b_i \\ 0 & 0 \end{bmatrix} \tag{22}$$

where variables are defined as in *Theorem 1* and $\boldsymbol{m}$ is determined based on the intermediate variable $(\hat{\boldsymbol{m}}_j)$ which is defined as follows:

$$\boldsymbol{m} = \frac{\hat{\boldsymbol{m}}_j}{\boldsymbol{\theta}_j}. \tag{23}$$

The proof of the *Theorem 2* is similar to *Theorem 1* and is not presented here.

D. Design Procedure

The design procedure is shown in a flowchart form in Fig. 6. The transient and steady-state responses of the system are considered as performance specifications. The main transient specifications are rise time, the start-up percentage of overshoot,

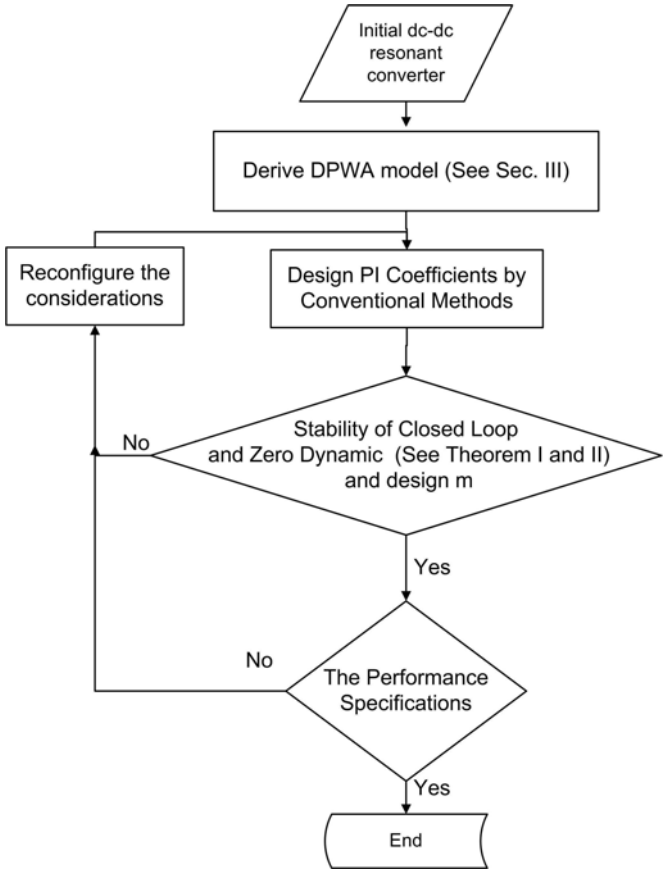

Fig. 6. Design flowchart for proposed control strategy.

and dynamic response for load and line regulation. If the performance specifications are not met by the designed controller, the initial considerations must be reconfigured for the design in the next step. k_I, k_P, and α_i must be initialized again for the next step design. The dc offset gain and slope of switching surface image on $x_1 - x_2$ plane are designed by the proposed procedure. Considering Fig. 5, the design parameters are the dc offset of switching surface m and the PI controller coefficients in the inner and the outer control loops, respectively. Then, the PI coefficients are designed by conventional methods such as Ziegler–Nichols method. Finally, the closed loop stability analysis and design of m may be performed by the presented *Theorem 1* and the minimum phase attribute is verified by *Theorem 2*.

E. Comparison of Hybrid Control Methods

Different hybrid modeling and control methods have been presented for power electronic converters. A good comparison is presented in [19] for hybrid control strategies and their implementation methods. Table III compares the proposed method with other hybrid methods. The proposed method has low complexity of implementation and can be simply implemented by analog or digital circuits. It does not use any modulator.

TABLE III
COMPARISON OF HYBRID CONTROL METHODS FOR POWER ELECTRONIC CONVERTERS

Control Method	Modulator	Implementation Complexity	Stability Analysis
Adaptive-predictive control approach [20]	PWM	high	hard
Explicit model predictive control [21]	PWM	high	hard
Sampled data control for robust tracking [22]	PWM	high	hard
Stabilizing control approach [23]	No Need	low	very simple
Hybrid-Flatness Approach [7]	No Need	low	very simple
Direct Piece-Wise Affine approach	No Need	low	simple

TABLE IV
PARAMETERS OF DC–DC SERIES RESONANT CONVERTER

Symbol	Parameter	Value
C	tank capacitor	$560nF$
L	tank inductor	$14.7\mu H$
C_f	output capacitor	$47\mu F$
V_g	input voltage	$48V$
V_o	output voltage	$20V$
ω_s	angular switching frequency	$100kHz$
ω_r	angular resonant frequency	$54kHz$
R	output resistance	6Ω
V_f	forward voltage of diodes	1.25
r_{Loss}	the sum effect of the inductor resistance and the capacitor series resistance	0.76Ω

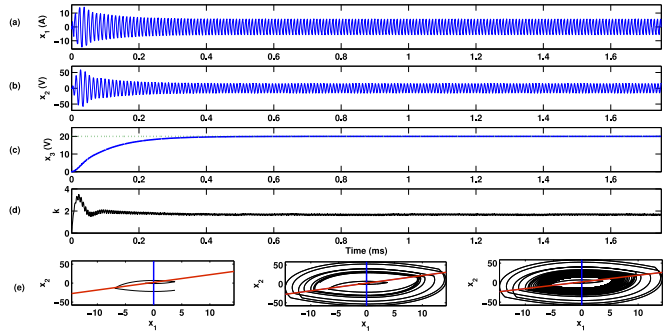

Fig. 7. Simulated start-up waveforms of SRC by the proposed control, (a) tank inductor current, (b) tank capacitor voltage, (c) output capacitor voltage, (d) slope of switching surface image on $x_1 - x_2$ plane, (e) state plane with boundaries at three different times.

V. SIMULATION RESULTS

A dc–dc SRC is simulated for verification of the proposed method. The specifications and design values of the major components of the converter are summarized in Table IV. It is designed to work above resonance frequency.

The main transient specifications are rise time $t_r < 0.3$ ms, the start-up percentage of overshoot $P.O. < 20\%$, and the falling or rising times of the output voltage for load and supply variations < 0.3 ms. The waveforms of start-up is shown in Fig. 7. As it can be seen the soft start of the converter is an innate outcome of the adaptiveness of DPWA controller. In Fig. 7, the state plane with initial and designed boundaries is

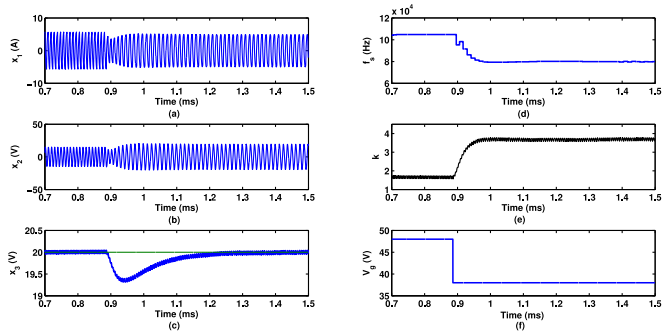

Fig. 8. Simulated waveforms of input voltage variation of SRC by the proposed control, (a) tank inductor current, (b) tank capacitor voltage, (c) output capacitor voltage, (d) switching frequency, (e) slope of designed switching line, (f) input voltage variation.

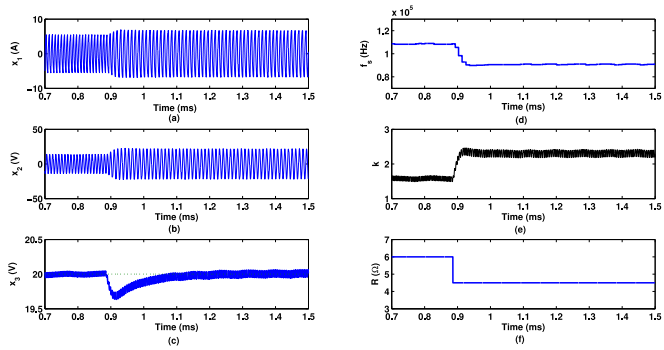

Fig. 9. Simulated waveforms of load variation of SRC by the proposed control, (a) tank inductor current, (b) tank capacitor voltage, (c) output capacitor voltage, (d) switching frequency (e) slope of designed switching line, (f) load resistance variations.

shown. The state trajectory switches among the regions which are enclosed by the presented boundaries. The bandwidth of the inner loop is higher than loop signal variations and so higher than switching frequency 100 kHz. The output of the outer loop is the output voltage and as can be seen in Fig. 7 is seen that the time-constant of output voltage 0.09 ms. The dominant pole of system is located at $1/0.00009$ and the approximate bandwidth of the outer control loop is 11 krad/s. Finally, it can be seen a bandwidth of 11 krad/s for the closed loop system, a rise time of $t_r = 0.23$ ms and a start-up percentage of overshoot $P.O. = 0$ is achieved.

The output voltage regulation at the presence of input voltage disturbance and load change are shown in Figs. 8 and 9, respectively. The variations of the tank inductor current and the tank capacitor voltage are shown simultaneously with the output voltage in Figs. 8 and 9. In Fig. 8, the input voltage varies from 48 to 38 V and the output voltage is regulated in 0.35 ms. In Fig. 9, the load resistance is arbitrarily changed from 6 to 4.5 Ω and one can see that the output voltage is regulated in about 0.29 ms. The switching frequency and the slope of the designed switching boundary are also depicted in these figures. The variations of the switching frequency demonstrates that the control effort of the proposed controller and the feasibility of the converter for implementation of power semiconductors. According to the presented results, the effectiveness of the proposed control strategy is obvious.

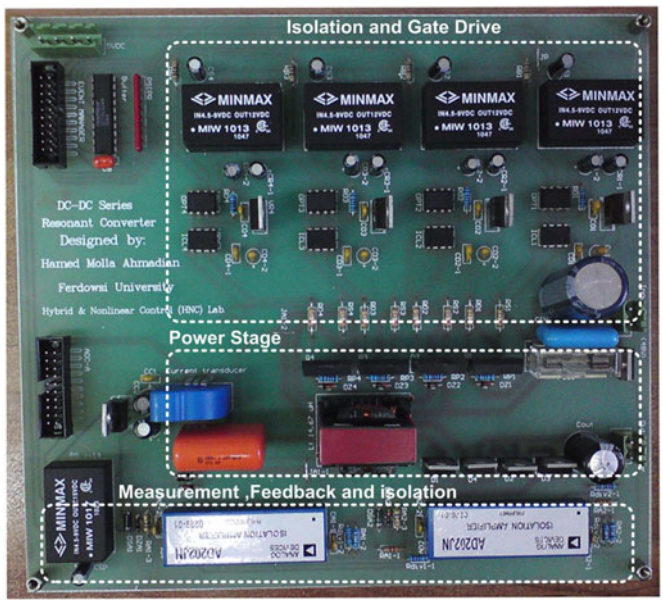

Fig. 10. Experimental dc–dc SRC with name of three main sections.

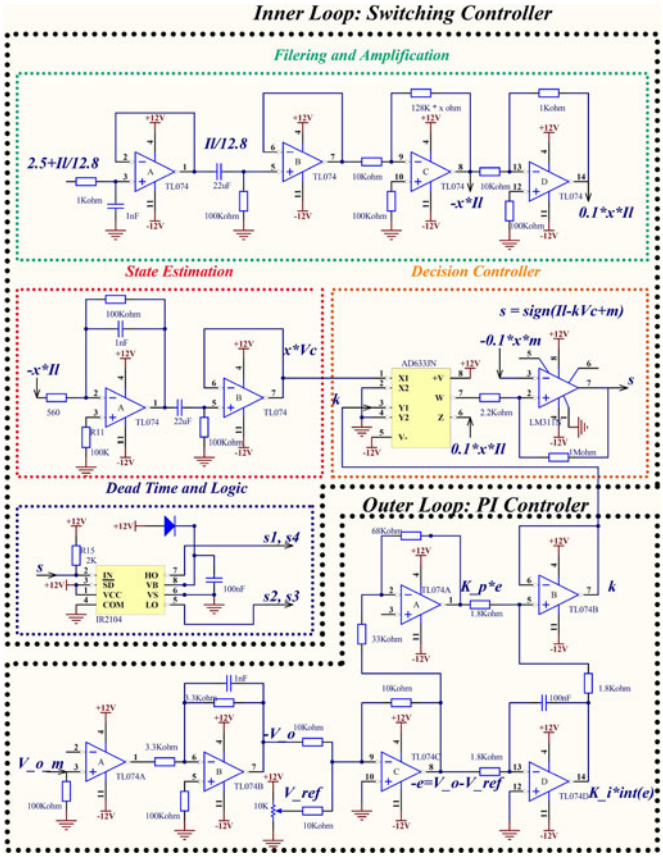

Fig. 11. Circuit diagram of the DPWA controller showing names of the sections and signals.

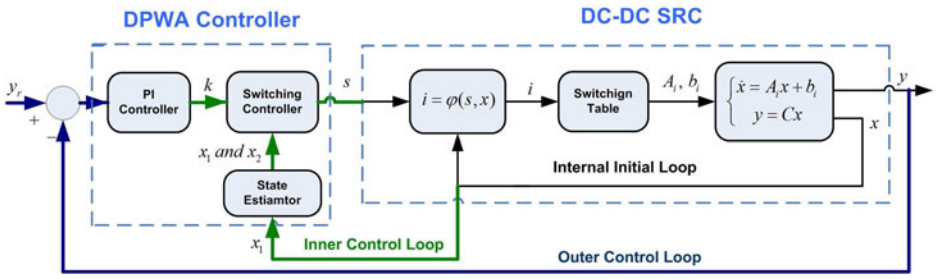

Fig. 12. Block diagram of hybrid control for SRC with state estimator.

VI. Experimental Implementation and Results

For better verification of proposed control strategy, an experimental prototype was designed and implemented. Fig. 10 shows the designed resonant converter. The experimental prototype consists of three different sections; 1-isolation and gate drive, 2-power stage and 3-measurement, feedback and isolation. The fast operation of switched controller is hard for digital implementation. Consequently, an analog technique is selected for this implementation as shown in Fig. 11. The inner control loop is an adaptive switched controller which is made of four sections that are denoted in this figure. A filtering and amplification section has the role of signal scaling and noise rejection. The estimation of tank capacitor voltage is done by the section of state estimation and decision controller. The output of switched controller must be converted to suitable switching signals for PMOSs with an appropriate dead time. This conversion is done by dead time and logic section. The outer control loop is the PI controller and is implemented by operational amplifiers.

In order to apply the proposed control strategy, as shown in the block diagram of the Fig. 5, a high-frequency isolated voltage sensor is necessary. Using a high-frequency isolated voltage sensor is not practically feasible for the implementation of the converter. Therefore, a state estimator is used as a solution that is shown in the block diagram of Fig. 12. The verification of the proposed estimation method is shown in Fig. 13. In this figure, the estimated and the actual values of the tank capacitor voltage are shown.

The experimental results of output voltage are shown in Figs. 14 and 15 for input voltage and load change variations, respectively. The disturbance rejection of the proposed control method is validated by the input voltage variation from 48 to 38 V at $t = 1$ ms in Fig. 14. The output voltage is compensated in 0.37 ms. The robustness in front of uncertainty in the proposed method is validated by the load variation from $6\ \Omega$ to $4.5\ \Omega$ at $t = 0.27$ ms in Fig. 15. The output voltage is compensated in 0.22 ms. Good voltage stability and small transient response of experimental results are obvious.

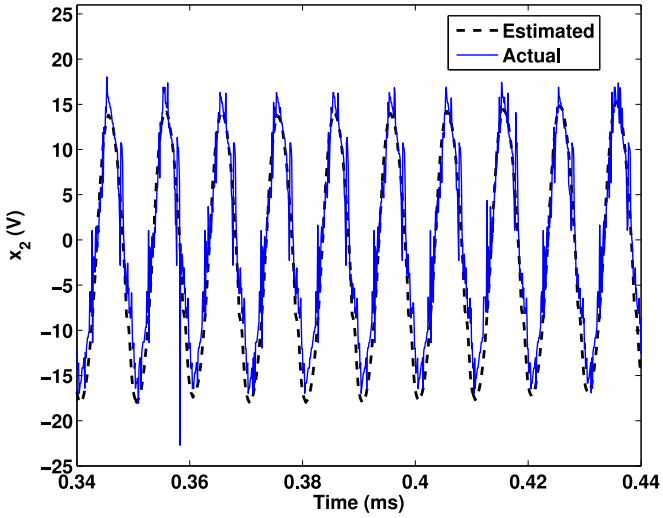

Fig. 13. Actual and estimated value of tank capacitor voltage in steady-state operation of SRC.

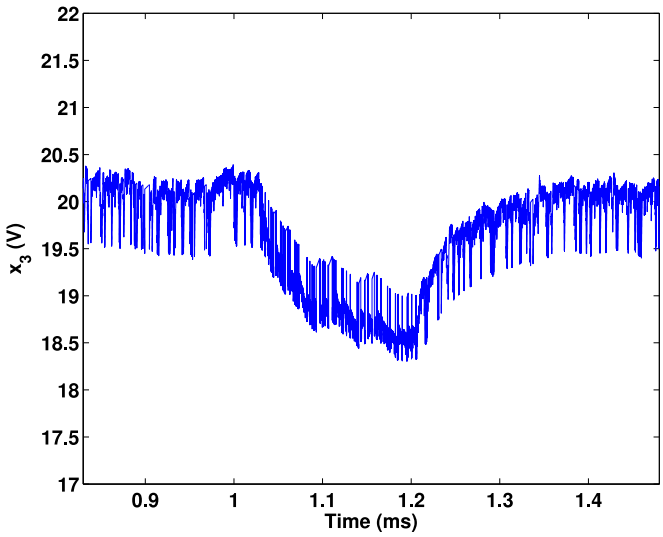

Fig. 14. Output voltage of SRC for stepwise input voltage change from 48 to 40 V at $t = 1$ ms.

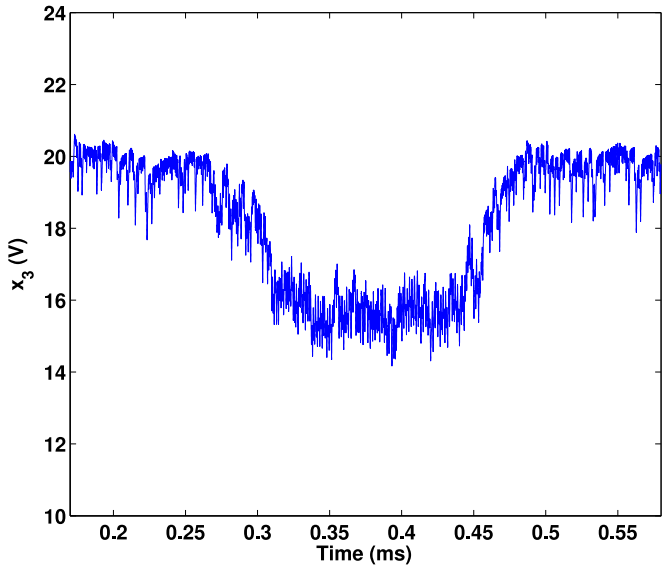

Fig. 15. Output voltage of SRC for stepwise load change from 6 to $4.5\,\Omega$ at $t = 0.27$ ms.

VII. Conclusion

In this paper, for the stability analysis and control of resonant convertors, a novel hybrid control was presented. The proposed hybrid DPWA modeling and control was investigated for SRC. The hybrid DPWA control is based on nonaveraged large signal scheme. In order to analyze the stability of the proposed control and its zero dynamic, appropriate theorems were derived. The experimental and simulation results showed that the proposed control method has suitable steady state and transient response. It can be used for modeling, stability analysis, and controller design of other power electronic converters.

Appendix
Proof of Theorem

The augmented plant is a combination of plant and controller which is described by ellipsoidal DPWA model as

$$\begin{cases} \dot{x} = A_i x + b_i, & x \in \Omega_i \\ \dot{z} = y_{\text{ref}} - Cx, & z \in R \end{cases}$$

$$\Omega_i = \bigcap_{j=1}^{p_i} \{\, x \in R^n \mid ([\, k_I\, z + k_P(y_{\text{ref}} - Cx) \;\; -1 \;\; 0\,] + h_{ij}^T)x \,\} - g_{ij} - m < 0\}$$

and it can be shown in matrix form as

$$\begin{bmatrix} \dot{x} \\ \dot{z} \\ 0 \end{bmatrix} = A_{\text{aug},i} \begin{bmatrix} x \\ z \\ 1 \end{bmatrix}, \quad \begin{bmatrix} x \\ z \\ 1 \end{bmatrix} \in \Omega_i$$

$$A_{\text{aug},i} = \begin{bmatrix} A_i & 0 & b_i \\ -C & 0 & y_{\text{ref}} \\ 0 & 0 & 0 \end{bmatrix}.$$

For stability analysis, the following Lyaponouv function is considered:

$$V(x,z) = [\, x^T \quad z^T \quad 1\,]\, P \begin{bmatrix} x \\ z \\ 1 \end{bmatrix}$$

and from Lyaponouv theorem, the sufficient condition for stability and convergent rate of α_i is

$$\mathbf{0} < \boldsymbol{P}, A_{\text{aug},i}^T \boldsymbol{P} - \boldsymbol{P} A_{\text{aug},i} < -\alpha_i \boldsymbol{P}.$$

Using S-procedure and mentioned equations, the stability conditions are derived as

$$A_{\text{aug},i}^T \boldsymbol{P} + \boldsymbol{P} A_{\text{aug},i} + \alpha_i \boldsymbol{P} - \sum_{j=1}^{p_i} \boldsymbol{\theta}_j \begin{bmatrix} -C^T\,[1 \;\; 0 \;\; 0] & 0 & 0 \\ k_I\,[1 \;\; 0 \;\; 0] & 0 & 0 \\ k_P\, y_{\text{ref}}\,[1 \;\; 0 \;\; 0] - [0 \;\; 1 \;\; 0] + h_{ij}^T & 0 & -g_{ij} - \boldsymbol{m} \end{bmatrix} < 0.$$

The derived equation is BMI, we define $\hat{\boldsymbol{m}}_j = \boldsymbol{\theta}_j \boldsymbol{m}$, then

$$A_{\text{aug},i}^T \boldsymbol{P} + \boldsymbol{P} A_{\text{aug},i} + \alpha_i \boldsymbol{P} + \sum_{j=1}^{p_i} \begin{bmatrix} 0 & 0 & 0 \\ 0 & 0 & 0 \\ 0 & 0 & \hat{\boldsymbol{m}}_j \end{bmatrix} - \sum_{j=1}^{p_i} \boldsymbol{\theta}_j \begin{bmatrix} -C^T\,[1 \;\; 0 \;\; 0] & 0 & 0 \\ k_I\,[1 \;\; 0 \;\; 0] & 0 & 0 \\ k_P\, y_{\text{ref}}\,[1 \;\; 0 \;\; 0] - [0 \;\; 1 \;\; 0] + h_{ij}^T & 0 & -g_{ij} \end{bmatrix} < 0.$$

The final equation is in the LMI form. The Lyapunov function is satisfied on R^n hence the stability is global and the proof is complete.

References

[1] S. E. Lyshevski, "Resonant converters: Nonlinear analysis and control," *IEEE Trans. Ind. Elec.*, vol. 47, no. 4, pp. 751–758, Aug. 2000.
[2] F. Giri, O. E. Maguiri, H. E. Fadil, and F. Z. Chaoui, "Nonlinear adaptive output feedback control of series resonant dc-dc converters," *Control Eng. Pract.,* no. 19, pp. 1238–1251, 2011.
[3] V. M. Hernandez, R. Silva, and H. Sira-Ramirez, "On the stability of limit cycles in resonant DC-to-DC power converters," in *Proc. IEEE 42nd Conf. Decis. Control,* Dec. 9–12, 2003 pp. 1141–1146.
[4] F. Tahami and B. Molaei, "Piecewise affined system modeling and control of PWM converters," *J. Circuits, Syst., Comput.*, vol. 16, no. 1, pp. 113–128, Feb. 2007.
[5] F. Tahami, S. Poshtkouhi and H. Molla-Ahmadian, "Piecewise affine control design for power factor correction rectifiers," *J. Power Electron.*, vol. 11, no. 3, pp. 327–334, May 2011.
[6] A. Nejadpak and F. Tahami, "Stabilizing controller design for quasi-resonant converters described by a class of piecewise linear models," *IEEE Trans. Circuits Syst. I: Reg. Papers*, vol. 61, no. 1, pp. 312–323, Jan. 2014.
[7] H. Sira-Ramirez and R. Silva-Ortega, "On the control of the resonant converters: A hybrid flatness approach," presented at the Int. Symp. Math. Theory Netw. Syst., vol. 1, University of Notre Dame, Notre Dame, IN, USA, Aug. 12–16, 2002, pp. 1–15.
[8] W. Zhang, Y. Hou, X. Liu, and Y. Zhou, "Switched control of three-phase voltage source PWM rectifier under a wide-range rapidly varying active load," *IEEE Trans. Power Electron.*, vol. 27, no. 2, pp. 881–890, Feb. 2012.
[9] C. Olalla, I. Queinnec, R. Leyva, and A. E. Aroudi, "Optimal state-feedback control of bilinear DC–DC converters with guaranteed regions of stability," *IEEE Trans. Ind. Electron.*, vol. 59, no. 10, pp. 3868–3880, Oct. 2012.

[10] S. Maity and Y. Suraj, "Analysis and modeling of an fffhc-controlled DC–DC buck converter suitable for wide range of operating conditions," *IEEE Trans. Power Electron*, vol. 27, no. 12, pp. 4914–4924, Dec. 2012.
[11] W. Feng, F. C. Lee, and P. Mattavelli, "A hybrid strategy with simplified optimal trajectory control for LLC resonant converters," in *Proc. IEEE 27th Annu. Appl. Power Electron. Conf. Expo.*, Orlando, FL, USA, Feb. 5–9, 2012, pp. 1096–1103.
[12] H. Molla-Ahmadian, A. Karimpour, N. Pariz, and F. Tahami, "Hybrid modeling of a DC–DC series resonant converter: Direct piecewise affine approach," *IEEE Trans. Circuits Syst. I: Regular Papers*, vol. 59, no. 12, pp. 3112–3120, Dec. 2012.
[13] R. A. DeCarlo, M. S. Branicky, S. Pettersson, and B. Lennartson, "Perspectives and results on the stability and stabilizability of hybrid systems," *Proc. IEEE*, vol. 88, no. 7, pp. 1069–1082, Jul. 2000.
[14] A. Hassibi, S. P. Boyd, and J. P. How, "A class of Lyapunov functionals for analyzing hybrid dynamical systems," presented at the Amer. Control Conf., San Diego, CA, USA, Jun. 1999, vol. 4, pp. 2455–2460.
[15] L. Rodrigues, "Dynamic output feedback controller synthesis for piecewise affine systems," Ph.D. dissertation, Stanford Univ., Stanford, CA, USA, Jun. 2002.
[16] Hassibi, and S. Boyd, "Quadratic stabilization and control of piecewise-linear systems," *Proc. Amer. Control Conf.*, Jun. 24–26, 1998, pp. 3659–3664.
[17] J.-J. Slotine and W. Li, *Applied Nonlinear Control*. Englewood Cliffs, NJ, USA: Prentice-Hall, 1991.
[18] H. Sira-Ramirez, and R. Silva-Ortigoza, *Control Design Techniques in Power Electronics Devices*. New York, NY, USA: Springer-Verlag, 2006.
[19] S. Mariéthoz, S. Almer, M. Baja, A. G. Beccuti, D. Patino, A. Wernrud, J. Buisson, H. Cormerais, T. Geyer, H. Fujioka, U. T. Jonsson, C.-Y. Kao, M. Morari, G. Papafotiou, A. Rantzer, and P. Riedinger, "Comparison of hybrid control techniques for buck and boost DC–DC converters," *IEEE Trans. Control Syst. Technol.*, vol. 18, no. 5, pp. 1126–1145, Sep. 2010.
[20] D. Patino, P. Riedinger, and C. Iung, "Practical optimal state feedback control law for continuous-time affine switched systems with cyclic steady state," *Int. J. Control*, vol. 82, pp. 1357–1376, 2009.
[21] A. Beccuti, S. Mariethoz, S. Cliquennois, S. Wang, and M. Morari, "Explicit model predictive control of DC–DC switched mode power supplies with extended Kalman filtering," *IEEE Trans. Ind. Electron.*, vol. 56, no. 3, pp. 1864–1874, Jun. 2009.
[22] H. Fujioka, C.-Y. Kao, S. Almér, and U. Jönsson, "LQ optimal control for a class of pulse width modulated systems," *Automatica*, vol. 43, no. 6, pp. 1009–1020, 2007.
[23] J. Buisson, H. Cormerais, and P. Richard, "On the stabilization of switching electrical power converters," *Hybrid Syst.: Comput. Control*, vol. 3414, pp. 184–197, 2005.

Hamed Molla-Ahmadian was born in Mashhad, Iran, in 1982. He received the B.S. degree in electrical engineering from the Ferdowsi University of Mashhad, Mashhad, Iran, in 2004, the M.S. degree in electrical engineering from the Sharif University of Technology, Tehran, Iran, in 2007, and the Ph.D. degree in electrical engineering from Ferdowsi University of Mashhad, in 2012.

In 2007, he joined Khorasan Institute of Higher Education, Mashhad, Iran, where he is currently an Assistant Professor. Since 2008, he has been the Entrepreneur and the Chairman of Tajhizat Abzarazma Co, Mashhad, Iran. His research interests include the hybrid and switched systems, modeling and control of power electronic converters, and process systems engineering.

Farzad Tahami (M'97–SM'12) received the B.S. degree in electrical engineering from Ferdowsi University of Mashhad, Mashhad, Iran, in 1991, and the M.S. and Ph.D. degrees in electrical engineering from the University of Tehran, Tehran, Iran, in 1993 and 2003, respectively.

From 1991 to 2004, he was with R&D Department of Jovain Electrical Machines Corporation (JEMCO), Iran. In 2004, he joined Sharif University of Technology, Tehran, Iran, where he is currently an Associate Professor. Since 2007, he has been the Chairman of the technical committee of rotating machinery, The Iranian National Electrotechnical Committee (INEC).

Dr. Tahami is a Member of the Board of Directors and the Chairman of the education committee of the Power Electronics Society of Iran (PESI). His current research interests include electric motor drives, modeling and control of power electronic converters, soft switching, resonant converters, and vehicle system dynamics.

Ali Karimpour was born in Mashhad, Iran, in 1964. He received the B.Sc. and M.Sc. degrees in electrical engineering from the Ferdowsi University of Mashhad, Mashhad, Iran, in 1987 and 1990, respectively. He received the Ph.D. degree in electrical engineering from Ferdowsi University of Mashhad.

He is currently working as an Associate Professor at the Ferdowsi University of Mashhad. His research interests include multivariable control, hybrid systems, renewable energies, power system stability, and control structure design in power systems.

Naser Pariz received the B.Sc. (Hons.) and M.Sc. (Hons.) degrees in electrical engineering from the Ferdowsi University of Mashhad, Mashhad, Iran, in 1988 and 1991, respectively. He received the Ph.D. degree from the Department of Electrical Engineering, Ferdowsi University of Mashhad, in 2001.

He was a Lecturer at Ferdowsi University of Mashhad from 1991 to 1995, where he is currently a Professor. His research interests include nonlinear control and identification, hybrid systems, optimal control, power systems dynamics, and applied mathematics.